Original Article

The diagnostic, prognostic, drug sensitivity and ceRNA internet of *PPP4R1* in liver hepatocellular carcinoma (LIHC)

Xiaowei Li[1#], Yinglian Pan[1,2#], Siren Feng[1#], Weimei Xing[1], Bo Lin[1], Wei Li[1], Mengsen Li[1,3,4], Mingyue Zhu[1]

[1]Hainan Provincial Key Laboratory of Carcinogenesis and Intervention, Hainan Medical College, Haikou, China; [2]Department of Medical Oncology, First Affiliated Hospital, Hainan Medical College, Haikou, China; [3]Department of Medical Oncology, Second Affiliated Hospital, Hainan Medical College, Haikou, China; [4]Institution of Tumor, Hainan Medical College, Haikou, China

Contributions: (I) Conception and design: M Li, M Zhu; (II) Administrative support: M Zhu; (III) Provision of study materials or patients: Y Pan; (IV) Collection and assembly of data: X Li, S Feng, W Xing, B Lin, W Li; (V) Data analysis and interpretation: X Li; (VI) Manuscript writing: All authors; (VII) Final approval of manuscript: All authors.

[#]These authors contributed equally to this work as co-first authors.

Correspondence to: Mengsen Li, PhD. Hainan Provincial Key Laboratory of Carcinogenesis and Intervention, Hainan Medical College, 3 Xueyuan Road, Longhua District, Haikou 571199, China; Department of Medical Oncology, Second Affiliated Hospital, Hainan Medical College, Haikou, China; Institution of Tumor, Hainan Medical College, Haikou, China. Email: mengsenli@163.com; Mingyue Zhu, PhD. Hainan Provincial Key Laboratory of Carcinogenesis and Intervention, Hainan Medical College, 3 Xueyuan Road, Longhua District, Haikou 571199, China. Email: mingyuezhu2002@163.com.

Background: Recent studies have reported a role of protein phosphatase 4 regulatory subunit 1 (*PPP4R1*) in cancer development. However, its expression, diagnostic significance, prognostic value and biological function in liver hepatocellular carcinoma (LIHC) are not known.

Methods: The expression level of *PPP4R1* in pan-cancer was evaluated by analyzing publicly accessible data from the University of California Santa Cruz (UCSC) Xena database. The diagnostic value of *PPP4R1* for tumors was assessed using receiver operating characteristic (ROC) curves, whereas the impact of *PPP4R1* on tumor prognosis was determined using Kaplan-Meier survival curves, and a prognostic model for LIHC was established using cox regression analysis. In addition, analysis of the correlation between *PPP4R1* and anti-cancer drugs using Spearman's correlation coefficient was carried out. Four databases, miRWalk (mRNA-miRNA interactions), MicroT-CDS (mRNA-miRNA interactions), LncBase (miRNA-lncRNA interactions) and Encyclopedia of RNA Interactomes (ENCORI), were used to predict the competitive endogenous RNA (ceRNA) regulatory network of *PPP4R1*. Finally, the expression of *PPP4R1* protein levels was verified using experiments.

Results: The findings indicated that the *PPP4R1* expression level in cancerous tissues was notably greater than in adjacent tissues (P<0.05). *PPP4R1* showed diagnostic significance for 14 tumors based on the ROC curves results area under the curve >0.7. Furthermore, the Kaplan-Meier survival plots demonstrated that *PPP4R1* exhibited prognostic significance for all five tumors (P<0.05). According to the cox regression analysis, LIHC patients' prognosis was independently influenced by pathological stage, M stage, and *PPP4R1* (P<0.05). The drug sensitivity analysis revealed a positive correlation between the expression level of *PPP4R1* and the half maximal inhibitory concentration (IC50) of fludarabine. Additionally, the ceRNA network prediction indicated that the FGD5 antisense RNA 1 (FGD5-AS1)–hsa-miR-22-3p–*PPP4R1* ceRNA network could potentially contribute to the progression of LIHC. The experimental results showed that the expression level of *PPP4R1* protein was higher in cancer tissues than in paracancerous tissues.

Conclusions: *PPP4R1* has diagnostic value in most cancers, and high expression of *PPP4R1* is associated with poor prognosis, drug resistance and natural killer cell-mediated toxicity, particularly in LIHC. Therefore, *PPP4R1* may be a prognostic biomarker and a potential target for immunotherapy in LIHC.

Keywords: Liver hepatocellular carcinoma (LIHC); protein phosphatase 4 regulatory subunit 1 (*PPP4R1*); prognosis; drug-sensitivity; competitive endogenous RNA regulatory network (ceRNA regulatory network)

Submitted Sep 19, 2023. Accepted for publication Jan 08, 2024. Published online Feb 26, 2024.
doi: 10.21037/tcr-23-1744
View this article at: https://dx.doi.org/10.21037/tcr-23-1744

Introduction

Protein phosphatase 4 regulatory subunit 1 (*PPP4R1*, also referred to as PP4R1), serves as the regulatory subunit of protein phosphatase 4 (PP4). The existing literature (1,2) suggests that targeted interference and inhibition of PP4 activity may have potential benefits for tumor immunotherapy. It has been shown that inhibition of PP4 activity enhances cisplatin sensitivity, reduces the DNA damage response, and hinders tumor growth and progression (3). Nevertheless, research on *PPP4R1* in the context of tumors remains limited.

Based on available reports, it has been observed that *PPP4R1* hinders activation of the nuclear factor kappa-B (NF-κB) pathway in T cells and T lymphocytes by interacting with tumor necrosis factor receptor-associated factor molecules (4,5). Moreover, *PPP4R1* has been found to enhance the migration and metastasis of non-small cell lung cancer (NSCLC) by binding to the high-mobility group A2 (HMGA2) (6). Furthermore, Xiang *et al.* demonstrated that long non-coding RNA (lncRNA) insulin growth factor 2 antisense (IGF2-AS) facilitates the progression of thyroid cancer by modulating the miR-500a-3p/*PPP4R1*/phospho-vascular endothelial growth factor receptor 2 (p-VEGFR2) signalling pathway (7). However, the specific role of *PPP4R1* in other cancers remains unclear, for example, liver hepatocellular carcinoma (LIHC).

In this study, exploring the expression profile, diagnostic and prognostic value of *PPP4R1* were explored in pan-cancer by R software. Analysis of the correlation between *PPP4R1* and 24 immune cells was performed. Additionally, RNA sequencing data and anti-cancer drug data were obtained from the CellMiner database (8) and were used to assess the correlation between *PPP4R1* and anti-cancer drugs using the R software. Furthermore, prediction and construction of the competitive endogenous RNA (ceRNA) network were done through online databases in LIHC. Finally, experiments were conducted to elucidate the expression of *PPP4R1* at both the tissue and cellular levels, as well as to ascertain the localization of *PPP4R1* within LIHC cells. We hypothesized that *PPP4R1* is a new biomarker for LIHC and may be a target for LIHC immunotherapy. We present this article in accordance with the MDAR and REMARK reporting checklists (available at https://tcr.amegroups.com/article/view/10.21037/tcr-23-1744/rc).

Highlight box

Key findings

- Protein phosphatase 4 regulatory subunit 1 (*PPP4R1*) may be a prognostic biomarker and a potential target for immunotherapy in liver hepatocellular carcinoma (LIHC).

What is known and what is new?

- LIHC has a high incidence but a poor prognosis.
- *PPP4R1* can predict the prognosis of LIHC.

What is the implication, and what should change now?

- The role of *PPP4R1* in LIHC needs further study.

Methods

Analysis of differential gene expression

RNA sequencing data and clinical data of 18,102 cases were downloaded from the University of California Santa Cruz (UCSC) Xena database (https://xenabrowser.net/datapages/) in August 2022, including 7,568 cases of Genotype-Tissue Expression (GTEx) normal data, 727 cases of The Cancer Genome Atlas (TCGA) paracancer data and 9,807 cases of TCGA tumour data; both GTEx normal data and TCGA paracancer data were included in the normal group, and TCGA tumour data were included in the tumour group. The analysis of *PPP4R1* expression between tumor samples and normal samples was performed using the ggplot2 package in R software (V4.2.1). The differences between the two groups of data were analyzed using the Wilcoxon rank-sum test. The threshold for statistical significance was established as $P<0.05$.

Diagnostic value analysis

The cancer diagnostic importance of *PPP4R1* was assessed by employing a receiver operating characteristic (ROC) curve. A low diagnostic value was indicated by an area under the curve (AUC) between 0.5 and 0.7, while an intermediate diagnostic value was indicated by an AUC between 0.7 and 0.9, and a high diagnostic value was indicated by an AUC greater than 0.9.

Survival analysis

The overall survival (OS) rate of cancer patients was assessed using Kaplan-Meier survival curves to examine the influence of *PPP4R1* expression. When hazard ratio (HR) >1, a higher level of *PPP4R1* expression was linked to a poorer prognosis, while when HR <1, a lower level of *PPP4R1* expression was linked to a poorer prognosis. The threshold for statistical significance was established as $P<0.05$.

Correlation between PPP4R1 expression levels and clinical factors

The samples were categorized into groups based on the median of *PPP4R1* expression values, distinguishing between high-expression and low-expression groups. Afterwards, the R software was utilized to examine the disparities in clinical variables between the two groups. The threshold for statistical significance was established as $P<0.05$.

Prognostic factors analysis

RNA sequencing data and clinical data for TCGA-LIHC were downloaded from the TCGA database (https://portal.gdc.cancer.gov), and prognostic data were obtained from a cell article (9). The R software was used to perform univariate cox regression analysis on clinical variables, including pathologic stage, M stage, *PPP4R1*, histologic grade. These variables that had a P value lower than 0.05 were subsequently incorporated into the multifactorial cox regression analysis. An independent prognostic factor for the cancer was considered when the P value was below 0.05.

Protein-protein interaction (PPI) network construction and Gene Ontology (GO) and Kyoto Encyclopedia of Genes and Genomes (KEGG) enrichment analysis

The identification of differentially expressed genes (DEGs) of *PPP4R1* in LIHC was conducted using R software, Volcano maps were used for visualization. The *PPP4R1* co-expression genes were screened using STRING data (10) with the following conditions: network type: full STRING network; network edge meaning: evidence; active interaction sources: text mining, experiments, databases and co-expression; minimum required interaction score: medium confidence (0.400); maximum number of interactors to be displayed: no more than 50 interactors. Visualisation of co-expressed genes was done by using cytoscape software. Subsequently, the GO and KEGG enrichment analyses of the co-expression genes were performed using the clusterProfiler R package (11).

Immune cell infiltration and gene correlation analysis

The correlation between *PPP4R1* and the 24 immune cells was investigated using R software and the single sample gene set enrichment analysis (ssGSEA) algorithm. Subsequently, the TISIDB (an integrated repository portal for tumor-immune system interactions) database (12) was used to identify immunoinhibitor related genes linked to *PPP4R1* and to generate a molecular correlation scatter plot.

Drug sensitivity analysis

RNA sequencing data and drug data were obtained from the CellMiner database. Subsequently, the correlation between genes and drugs was examined using the impute package and limma package in the R software. Additionally, a correlation scatterplot was generated using ggplot2 and ggpubr packages.

Prediction and construction of a ceRNA network for PPP4R1

The miRWalk (mRNA-miRNA interactions) database (13) and MicroT-CDS (mRNA-miRNA interactions)

database (14) were used to predict the miRNAs that targeted *PPP4R1*. Additionally, the Encyclopedia of RNA Interactomes (ENCORI) database (15) and LncBase (miRNA-lncRNA interactions) database (16) were used to predict lncRNAs with the ability to bind to miRNAs. Subsequently, the correlation between *PPP4R1* and miRNAs was analyzed using the TCGA-LIHC dataset. Only miRNAs that exhibited a negative correlation with *PPP4R1* were retained. Next, the correlation between miRNAs and lncRNAs was explored, with a focus on retaining lncRNAs that displayed a negative correlation with miRNAs. Finally, the obtained results were visualized using cytoscape software to enhance the precision of predictions, and an analysis was conducted to examine the correlation between *PPP4R1* and lncRNAs. The lncRNAs exhibiting the highest positive correlation coefficients with *PPP4R1* were chosen as definitive members of the regulatory network.

Tissue and cell

Nine liver cancer tissues and paracancerous tissue specimens obtained from the First Affiliated Hospital of Hainan Medical College. LX-2, HLE, Huh7, PLC, and HepG2 cells were purchased from Wuhan Procell Life Technology Co., Ltd. Cells were cultured in Dulbecco's modified eagle medium (DMEM) (Cat #C3113-0500, Viva cell, China) supplemented with 10% fetal bovine serum, (Cat #164210-50, Procell, China) 100 μg/mL penicillin, and 0.25 μg/mL streptomycin (Cat #15140-122, Gibco, United States). The cells were then incubated at 37 ℃ with 5% CO_2. Once the cell population reached 5×10^6, trypsin was used to digest the cells and extract total protein for western blotting experiments. Additionally, 5×10^4 cells were used for immunofluorescence.

Western blotting

LX-2, HLE, Huh7, PLC and HepG2 cells were collected and lysed in lysis buffer (Cat #C510003, Sangon Biotech, China) for 40 min, then centrifuged at 12,000 rpm for 15 min at 4 ℃, and the supernatant was taken as the total protein of the cells, and the concentration of the total protein was determined by using BCA Protein Concentration Assay Kit (Cat #P0009, Beyotime, China). About 20ug of cell lysates was taken for 12% sodium dodecyl sulphate-polyacrylamide gel electrophoresis, and the proteins were subsequently transferred to a polyvinylidene fluoride (PVDF) membrane. The PVDF membrane was washed three times using phosphate buffered solution (PBST) buffer and then it was closed in protein free rapid blocking buffer (Cat #PS108, Epizyme, China) for 15 min, and then the membrane was incubated with a 1:2,000 dilution of *PPP4R1* antibody (Cat #67392-1-Ig, Proteintech, China) and a 1:10,000 dilution of glyceraldehyde-3-phosphate dehydrogenase (GAPDH) antibody (Cat #10494-1-AP, Proteintech) at 4 ℃ overnight. The membranes were then incubated with HPR-conjugated secondary antibodies (Cat #SA00001-2, Proteintech) at 37 ℃ for 1 h. The membranes were incubated with enhanced chemiluminescence (ECL) substrate and detected on a luminescent device. Grey scale values were analysed using image J software to quantify the relative expression of the proteins.

Immunohistochemistry

The level of PPP4R1 protein was assessed in LIHC tissue specimens using immunohistochemistry. In brief, the formalin-fixed and paraffin-embedded LIHC tissue sections were deparaffinized in xylene and rehydrated in a series of ethanol solutions (100–50%) and into tape water. The sections in a citric buffer (pH 5.0) were subjected to the antigen repair in a microwave and then incubated in normal serum-PBS (1:20 dilution) at room temperature for 1 h and then with an anti-*PPP4R1* antibody (Cat #67392-1-Ig, Proteintech) at 4 ℃ overnight. The following day, the sections were washed with PBS thrice and further incubated with a secondary antibody (Cat #GB23301, Servicebio, China) at a dilution of 1:200 at room temperature for 1 h. After brief washing with PBS, the sections were incubated with a 3,3'-diaminobenzidine (DAB) kit (Cat #G1212, Servicebio) at room temperature in the dark for 10 min and then incubated with DAB solution and counterstained with hematoxylin and mounted with coverslips. The stained sections were then reviewed and scored under a light microscope (E100, Nikon, Japan). Mean density were analysed using image J software to quantify the relative expression of the proteins.

Immunofluorescence

The HLE, Huh7 and LX-2 cells were placed in confocal dishes (Cat #BS-15-GJM, biosharp, China) and cultured overnight in an incubator, on the second day, take out the cell dishes and discard the medium and wash it 2 times with PBS, fix the cells with paraformaldehyde for 30 min, then

wash 2 times with PBS, to block the non-specific signals, close it with the special sealing solution for 15 min and then wash it with PBS for 2 times, The *PPP4R1* antibody (Cat #67392-1-Ig, Proteintech) was incubated overnight at 4 ℃, on the third day, the *PPP4R1* antibody was recovered and incubated with the second antibody (Cat #SA00013-3, Proteintech) in the incubation room at 37 ℃ for 1 h after washing it 2 times with PBS, and then photographed by adding the 4',6-diamidino-2-phenylindole (DAPI) staining solution (Cat #C1006, Beyotime) and put into a laser confocal microscope for observation (LSM800, ZEISS, Germany).

Statistical analysis

Statistical software using R software (4.2.1). The chi-square test was used for count data and the independent samples T test was used for measurement data. The data of two groups satisfied normal distribution and homogeneity using T test, satisfied normal distribution did not satisfy homogeneity using welch *t*-test, and did not satisfy normal distribution using Wilcoxon rank sum test. Indicators with missing data ≥60% were excluded from the statistical analysis. $P<0.05$ was considered as statistically significant difference.

Ethical statement

The study was conducted in accordance with the Declaration of Helsinki (as revised in 2013). The study was approved by Ethics Committee of the First Affiliated Hospital of Hainan Medical College (No. 2023-KYS-161) and informed consent was taken from all the patients.

Results

Expression levels of PPP4R1 in pan-cancer

The expression level of *PPP4R1* in pan-cancer was investigated by analyzing the pan-cancer RNA sequencing dataset with R software. The analysis revealed that *PPP4R1* exhibited high expression in 11 tumors and low expression in 13 tumors in unpaired samples (*Figure 1A*). Furthermore, the analysis revealed that *PPP4R1* exhibited high expression in four tumors and only one tumor displayed low expression (*Figure 1B*) in paired samples. Through the integration of *PPP4R1* expression levels in tumor tissues and normal tissues, in both paired and unpaired samples, it was discovered that *PPP4R1* exhibited high expression exclusively in cholangiocarcinoma (CHOL) and LIHC, while displaying low expression in kidney chromophobe (KICH).

Diagnostic significance of PPP4R1 in pan-cancer

ROC curve analysis revealed that *PPP4R1* exhibited diagnostic value for 14 different types of cancer, with an AUC greater than 0.7. The specific AUC values for each cancer type were as follows: LIHC (AUC =0.867); colon adenocarcinoma (COAD) (AUC =0.786); CHOL (AUC =1.000); rectum adenocarcinoma (READ) (AUC =0.858); uterine carcinosarcoma (UCS) (AUC =0.822); KICH (AUC =0.860); brain lower grade glioma (LGG) (AUC =0.869); pancreatic adenocarcinoma (PAAD) (AUC=0.950); ovarian serous cystadenocarcinoma (OV) (AUC =0.876); adrenocortical carcinoma (ACC) (AUC =0.861); oral squamous cell carcinoma (OSCC) (AUC =0.774); skin cutaneous melanoma (SKCM) (AUC =0.882); glioblastoma multiforme (GBM) (AUC =0.888); and testicular germ cell tumors (TGCT) (AUC =0.953) (*Figure 2*). According to these results, *PPP4R1* has high diagnostic value in CHOL, PAAD, and TGCT (AUC >0.9), medium diagnostic value in LIHC, READ, UCS, KICH, LGG, OV, ACC, SKCM and GBM (AUC >0.8), low diagnostic value in COAD and OSCC (AUC >0.7).

Prognostic significance of PPP4R1 in pan-cancer

Kaplan-Meier survival curves for LIHC, PAAD, sarcoma (SARC), and ACC demonstrated a significant association between *PPP4R1* expression and OS in these cancer types. Specifically, high expression of *PPP4R1* was found to be indicative of poor prognosis in patients with LIHC (HR =1.64, P=0.006), PAAD (HR =1.66, P=0.019) and SARC (HR =1.51, P=0.043), as depicted in *Figure 3A-3C*. However, in kidney renal clear cell carcinoma (KIRC), *PPP4R1* was shown to be a protective factor for prognosis (HR =0.69, P=0.017) (*Figure 3D*). In *Figure 3E*, it is shown that *PPP4R1* was a poor prognostic factor for ACC (HR =3.29, P=0.004).

Association between PPP4R1 expression levels and different clinical features of LIHC

Based on our comprehensive analysis across multiple cancer types, it was observed that *PPP4R1* was significantly upregulated specifically in LIHC. Furthermore, *PPP4R1*

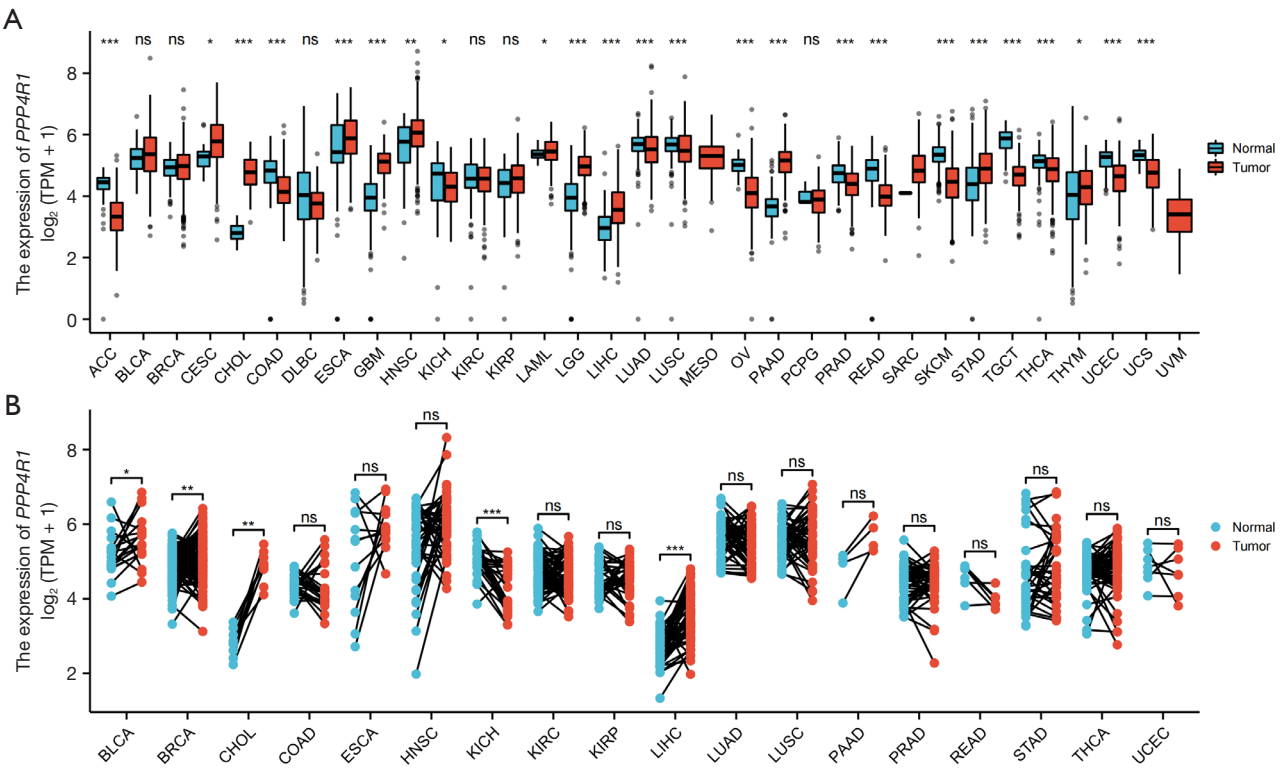

Figure 1 Expression of *PPP4R1* in pan-cancer. (A) Expression of *PPP4R1* in unpaired samples; (B) expression of *PPP4R1* in paired samples. ns, P≥0.05; *, P<0.05; **, P<0.01; ***, P<0.001. *PPP4R1*, protein phosphatase 4 regulatory subunit 1; TPM, transcripts per million; ns, no significance; ACC, adrenocortical carcinoma; BLCA, bladder urothelial carcinoma; BRCA, breast invasive carcinoma; CESC, cervical cancer; CHOL, cholangiocarcinoma; COAD, colon adenocarcinoma; DLBC, large b-cell lymphoma; ESCA, esophageal cancer; GBM, Glioblastoma multiforme; HNSC, Head and neck squamous cell carcinoma; KICH, kidney chromophobe; KIRC, Kidney renal clear cell carcinoma; KIRP, kidney papillary cell carcinoma; LAML, acute myeloid leukemia; LGG: brain lower grade glioma; LIHC, liver hepatocellular carcinoma; LUAD, lung adenocarcinoma; LUSC, lung squamous cell carcinoma; MESO, mesothelioma; OV, ovarian serous cystadenocarcinoma; PAAD, Pancreatic adenocarcinoma; PCPG, pheochromocytoma & paraganglioma; PRAD, prostate cancer; READ, rectum adenocarcinoma; SARC, sarcoma; SKCM, melanoma; STAD, stomach adenocarcinoma; TGCT, testicular germ cell tumors; THCA, thyroid cancer; THYM, thymoma; UCEC, uterine corpus endometrial carcinoma; UCS, uterine carcinosarcoma; UVM, uterine carcinosarcoma.

demonstrated diagnostic and prognostic potential exclusively in the context of LIHC. Consequently, our subsequent investigation primarily focused on elucidating the association between *PPP4R1* and LIHC. The baseline datasheet analysis revealed a statistically significant association between *PPP4R1* expression levels and various clinical factors in LIHC, including pathologic T stage (P=0.664), pathologic M stage (P=0.123), gender (P=0.097), age (P=0.008), pathological stage (P=0.024), histological grading (P=0.004) and alpha-fetoprotein (AFP) levels (P<0.001) (*Table 1*). Notably, patients with age (≤60 years), pathological stages (III and IV), histological grades (G3 and G4), and AFP levels (>400 ng/mL) exhibited increased *PPP4R1* expression levels (*Figure 4*).

Cox regression analysis—single and multiple factors

To explore the prognostic factors for *PPP4R1* in LIHC, cox regression analyses were performed. Univariate cox regression analysis revealed that pathological stage (HR =2.09, 95% CI: 1.429–3.055, P<0.001), M stage (HR =4.077, 95% CI: 1.281–12.973, P=0.017), and *PPP4R1* (HR =1.643, 95% CI: 1.157–2.335, P=0.006) were associated with poor prognosis in LIHC (*Table 2*). In the multivariate

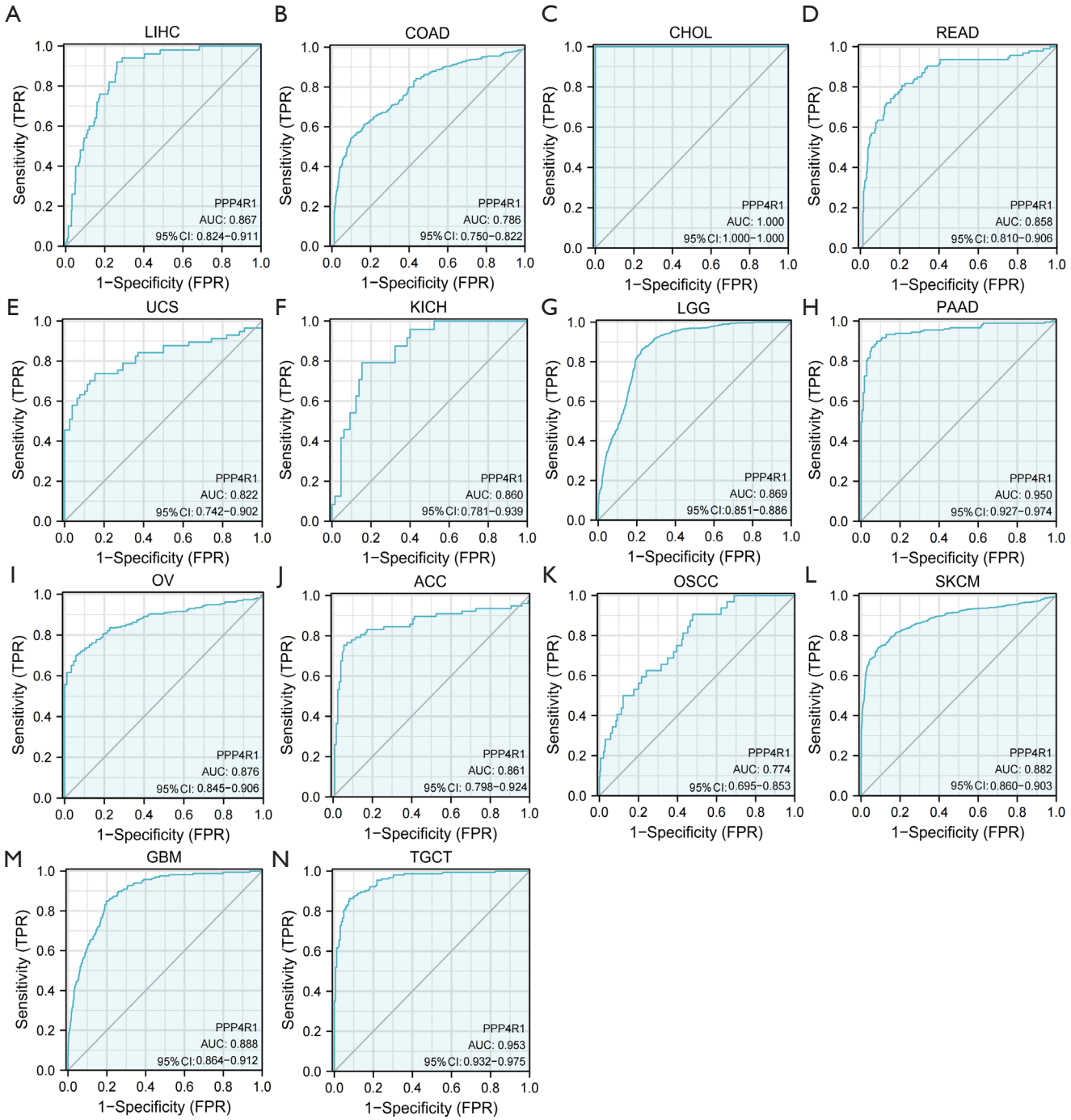

Figure 2 ROC curve of *PPP4R1* expression in pan-cancer. (A) LIHC; (B) COAD; (C) CHOL; (D) READ; (E) UCS; (F) KICH; (G) LGG; (H) PAAD; (I) OV; (J) ACC; (K) OSCC; (L) SKCM; (M) GBM; (N) TGCT. ROC, receiver operating characteristic; *PPP4R1*, protein phosphatase 4 regulatory subunit 1; LIHC, liver hepatocellular carcinoma; TPR, true positive rate; AUC, area under the curve; CI, confidence interval; FPR, false positive rate; COAD, colon adenocarcinoma; CHOL, cholangiocarcinoma; READ, rectum adenocarcinoma; UCS, uterine carcinosarcoma; KICH, kidney chromophobe; LGG, brain lower grade glioma; PAAD, pancreatic adenocarcinoma; OV, ovarian serous cystadenocarcinoma; ACC, adrenocortical carcinoma; OSCC, oral squamous cell carcinoma; SKCM, skin cutaneous melanoma; GBM, glioblastoma multiforme; TGCT, testicular germ cell tumors.

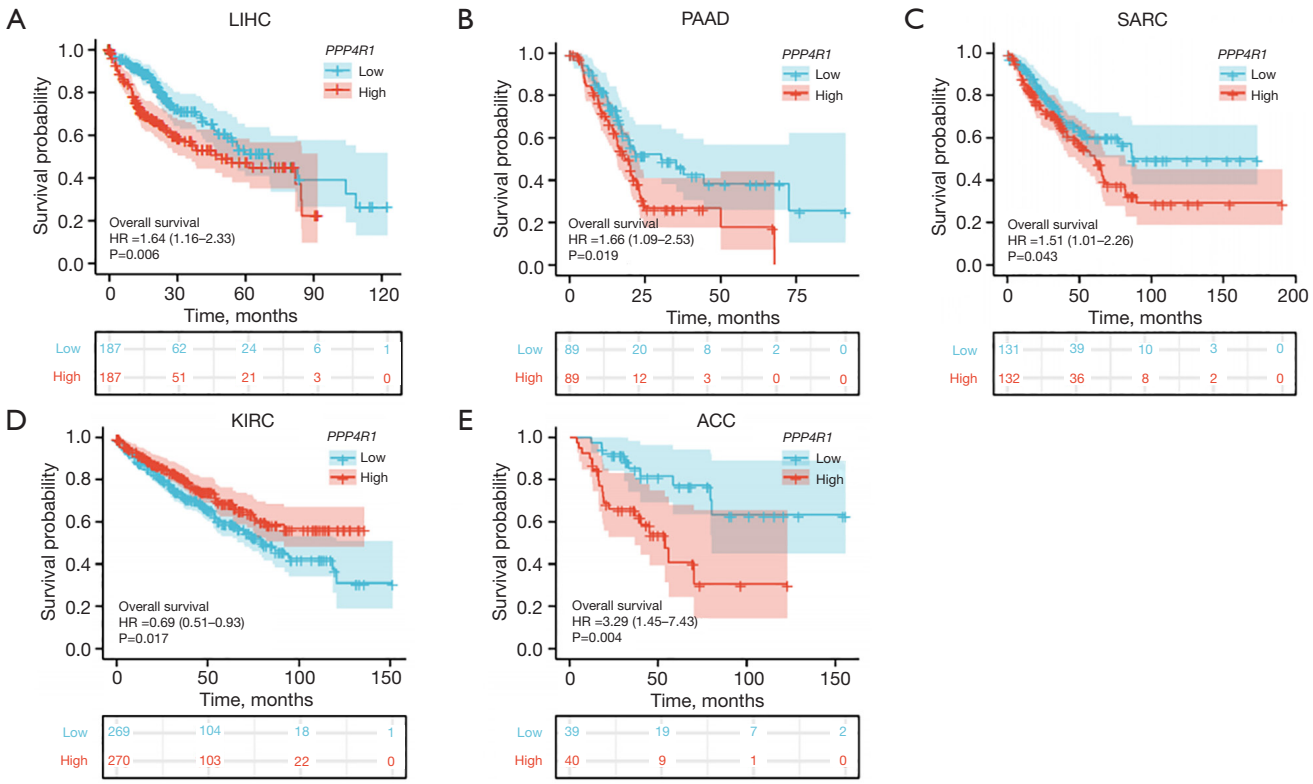

Figure 3 *PPP4R1* expression and prognosis of cancers. (A) LIHC; (B) PAAD; (C) SARC; (D) KIRC; (E) ACC. *PPP4R1*, protein phosphatase 4 regulatory subunit 1; LIHC, liver hepatocellular carcinoma; PAAD, pancreatic adenocarcinoma; SARC, sarcoma; KIRC, kidney renal clear cell carcinoma; ACC, adrenocortical carcinoma.

cox regression analysis, pathological stage (HR =2.504, 95% CI: 1.570–3.994, P<0.001), M stage (HR =3.865, CI: 1.164–12.826, P=0.027), and *PPP4R1* (HR =1.776, 95% CI: 1.131–2.787, P=0.013) were independent prognostic factors for the OS of LIHC patients (*Table 2*).

PPP4R1 differential expression analysis, PPI network construction and GO and KEGG enrichment analysis in LIHC

To investigate the biological function of *PPP4R1*, R software was used to screen the DEGs of *PPP4R1* in LIHC and the results were visualized by volcano plot (*Figure 5A*), then *PPP4R1* co-expression genes were explored using STRING database, and a total of 50 co-expression genes were obtained, which were visualised by cytoscape (*Figure 5B*). Finally, these 50 genes were analysed by GO and KEGG enrichment, and the results of GO enrichment analysis showed that the biological processes (BP) mainly included dephosphorylation, negative regulation of phosphate metabolism process, cell growth, mitotic cell cycle phase transition and calcineurin-NFAT signalling cascade; cellular components (CC) mainly included protein serine/threonine phosphatase complex, protein phosphatase type 2A complex, chromosome, centromeric region, spindle and glutamatergic synapse; molecular functions (MF) mainly included protein phosphatase regulator activity, phosphoric ester hydrolase activity, protein phosphatase binding, tau protein binding and cyclosporin A binding (*Figure 5C*). KEGG pathway enrichment was mainly associated with phosphatidylinositol 3-kinase (PI3K)-Akt signalling pathway, AMP-activated protein kinase (AMPK) signalling pathway, mRNA surveillance signalling pathway, Hippo signalling pathway, Wnt signalling pathway, programmed cell death-ligand 1 (PD-L1) expression and programmed cell death protein 1 (PD-1) checkpoint pathway in cancer, and NF-κB signalling pathway. In addition, KEGG enrichment was observed to associate *PPP4R1* with hepatitis C, cellular senescence and

Table 1 Relationship between clinical parameters and *PPP4R1* in patients with LIHC

Characteristics	Low expression of *PPP4R1* (N=187)	High expression of *PPP4R1* (N=187)	P value
Pathologic T stage, n (%)			0.664
T1	95 (25.4)	88 (23.5)	
T2	48 (12.8)	47 (12.6)	
T3	35 (9.4)	45 (12.0)	
T4	6 (1.6)	7 (1.9)	
Missing	3 (0.8)	0	
Pathologic M stage, n (%)			0.123
M0	130 (34.7)	138 (36.9)	
M1	4 (1.1)	0	
Missing	53 (14.2)	49 (13.1)	
Gender, n (%)			0.097
Female	53 (14.2)	68 (18.2)	
Male	134 (35.8)	119 (31.8)	
Age, n (%)			0.008
≤60 years	76 (20.3)	101 (27.0)	
>60 years	111 (29.7)	85 (22.7)	
Missing	0	1 (0.3)	
Pathologic stage, n (%)			0.024
Stage I	89 (23.8)	84 (22.5)	
Stage II	45 (12.0)	42 (11.2)	
Stage III	33 (8.8)	52 (13.9)	
Stage IV	5 (1.4)	0	
Missing	15 (4.0)	9 (2.4)	
Histologic grade, n (%)			0.004
G1	35 (9.4)	20 (5.3)	
G2	97 (25.9)	81 (21.7)	
G3	50 (13.4)	74 (19.8)	
G4	3 (0.8)	9 (2.4)	
Missing	2 (0.5)	3 (0.8)	
AFP, n (%)			<0.001
≤400 ng/mL	126 (33.7)	89 (23.8)	
>400 ng/mL	20 (5.3)	45 (12.0)	
Missing	41 (11.0)	53 (14.2)	

The significance level was set at P<0.05. *PPP4R1*, protein phosphatase 4 regulatory subunit 1; LIHC, liver hepatocellular carcinoma; AFP, alpha-fetoprotein.

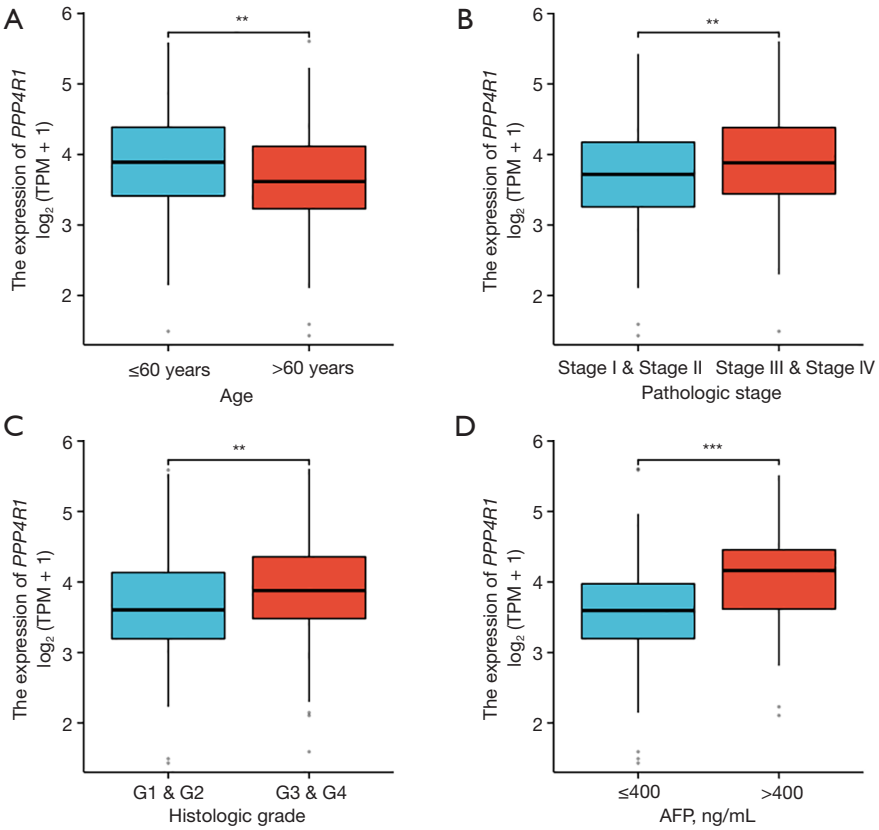

Figure 4 Box plots for *PPP4R1* expression and clinical features in LIHC. (A) Age; (B) pathologic stage; (C) histologic grade; (D) AFP. **, P<0.01; ***, P<0.001. *PPP4R1*, protein phosphatase 4 regulatory subunit 1; TPM, transcripts per million; AFP, alpha-fetoprotein; LIHC, liver hepatocellular carcinoma.

Table 2 Prognostic factors in LIHC patients analysed by univariate and multivariate cox regression

Characteristics	Total (N)	Univariate analysis		Multivariate analysis	
		Hazard ratio (95% CI)	P value	Hazard ratio (95% CI)	P value
Pathologic stage	349				
Stage I	173	Reference			
Stage II & III & IV	176	2.090 (1.429–3.055)	<0.001	2.504 (1.570–3.994)	<0.001
M stage	272				
M0	268	Reference			
M1	4	4.077 (1.281–12.973)	0.017	3.865 (1.164–12.826)	0.027
PPP4R1	374				
Low	187	Reference			
High	187	1.643 (1.157–2.335)	0.006	1.776 (1.131–2.787)	0.013
Histologic grade	368				
G1 & G2	233	Reference			
G3 & G4	135	1.091 (0.761–1.564)	0.636		

The significance level was set at P<0.05. LIHC, liver hepatocellular carcinoma; CI, confidence interval; PPP4R1, protein phosphatase 4 regulatory subunit 1.

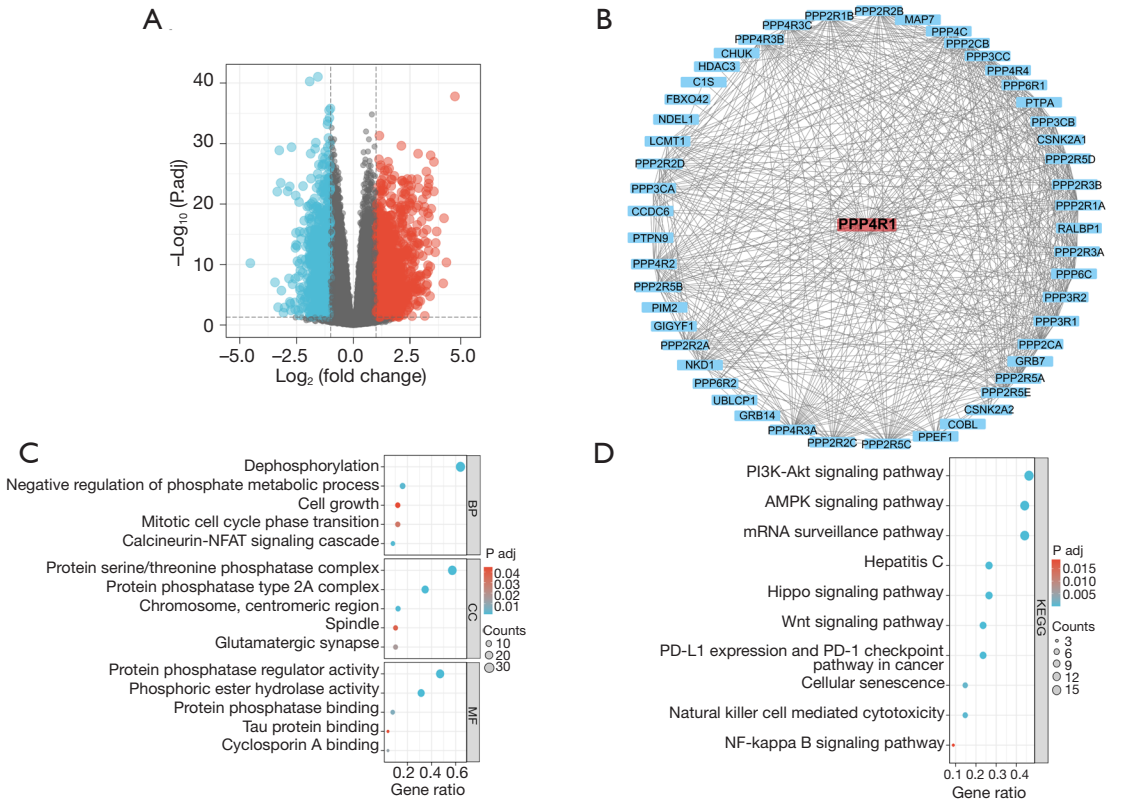

Figure 5 Differentially expressed genes of *PPP4R1*, PPI network and GO and KEGG enrichment analysis in LIHC. (A) Volcano plot of *PPP4R1* differentially expressed genes; (B) PPI network; (C) the GO enrichment analysis; (D) the KEGG enrichment analysis. BP, biological process; CC, cellular component; MF, molecular function; PI3K-Akt, phosphatidylinositol 3-kinase-Akt; AMPK, AMP-activated protein kinase; PD-L1, programmed death-ligand 1; PD-1, programmed death protein 1; NF, nuclear factor; *PPP4R1*, protein phosphatase 4 regulatory subunit 1; PPI, protein-protein interaction; GO, Gene Ontology; KEGG, Kyoto Encyclopedia of Genes and Genomes; LIHC, liver hepatocellular carcinoma.

natural killer (NK) cell-mediated cytotoxicity (*Figure 5D*).

Immune infiltration and gene correlation analysis

Using the R package, we employed the ssGSEA algorithm to investigate the correlation between *PPP4R1* and 24 different types of immune cells (*Figure 6A*). The results showed that *PPP4R1* had a strong positive relationship with Th2 cells, helper T cells, Tem, Tcm, macrophages, NK CD56bright cells and follicular helper T cell (TFH), with correlation coefficients (R-values) of 0.382 (P<0.001), 0.367 (P<0.001), 0.270 (P<0.001), 0.227 (P<0.001), 0.190 (P<0.001), 0.188 (P<0.001) and 0.156 (P<0.01), respectively. In addition, *PPP4R1* had a strong negative relationship with Th17 cells, with correlation coefficients (R-value) of –0.394 (P<0.001). Furthermore, the association between *PPP4R1* and genes related to immunoinhibitors was examined by utilizing the TISIDB database. The findings showed notable associations between *PPP4R1* and programmed cell death protein 1 (PDCD1), hepatitis A virus-cellular receptor 2 (HAVCR2), cytotoxic T lymphocyte antigen 4 (CTLA4), and transforming growth factor-beta1 (TGF-β1), with correlation coefficients of 0.19 (P<0.001), 0.172 (P<0.001), 0.153 (P=0.0031), and 0.22 (P<0.001), respectively (*Figure 6B-6E*).

Drug sensitivity analysis

Anti-cancer drugs are important in the treatment of cancer; however, resistance often develops during treatment, so it is crucial to study the relationship between genes and the sensitivity of anti-cancer drugs. As shown in *Figure 7*, the expression of *PPP4R1* was negatively correlated with the half maximal inhibitory concentration (IC50) values of

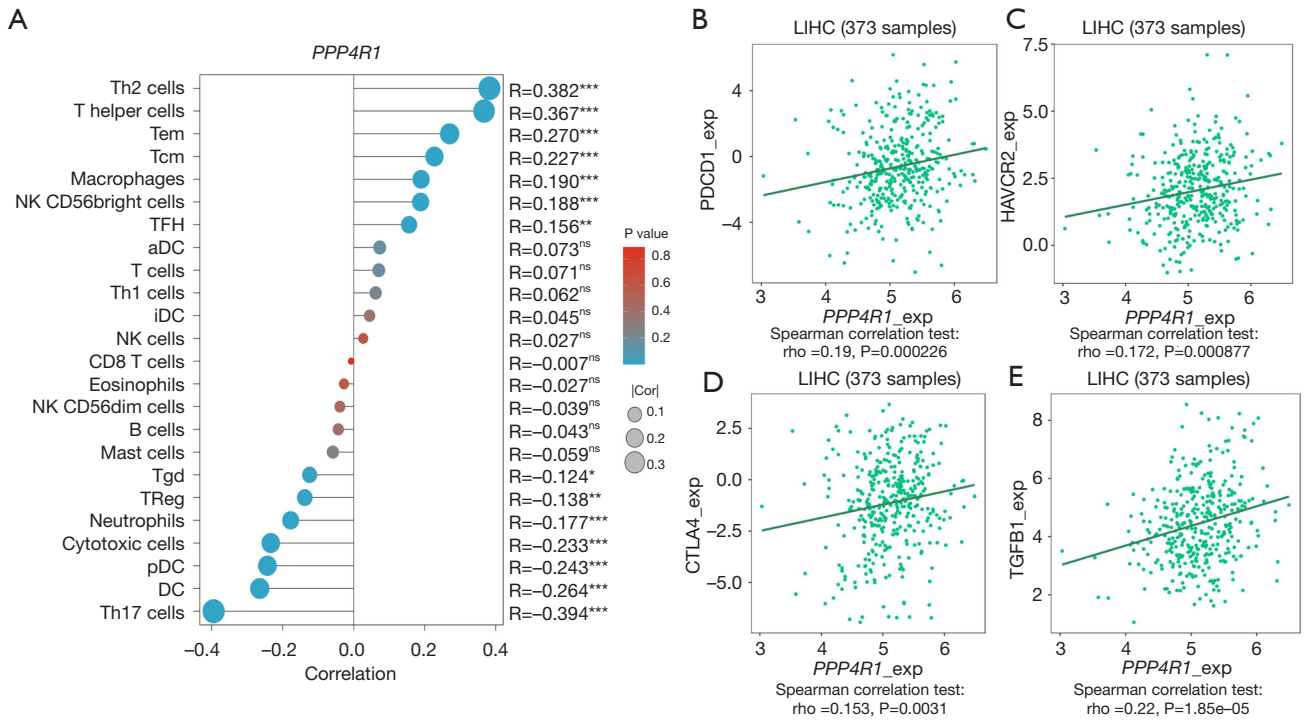

Figure 6 Relationship between *PPP4R1* expression levels in LIHC and immune cells and immunoinhibitor related genes. (A) Relevance lollipop chart of *PPP4R1* expression level and 24 immune cells; (B) correlation scatter diagram of *PPP4R1* and PDCD1; (C) correlation scatter diagram of *PPP4R1* and HAVCR2; (D) correlation scatter diagram of *PPP4R1* and CTLA4; (E) correlation scatter diagram of *PPP4R1* and TGFB1. ns, P≥0.05; *, P<0.05; **, P<0.01; ***, P<0.001. *PPP4R1*, protein phosphatase 4 regulatory subunit 1; LIHC, liver hepatocellular carcinoma; PDCD1, programmed cell death 1; HAVCR2, hepatitis A virus-cellular receptor 2; CTLA4, cytotoxic T lymphocyte antigen 4; TGFB1, transforming growth factor-beta1; NK, natural killer; TFH, follicular helper T cell; ns, no significance.

tamoxifen, actinomycin D, vemurafenib, ergenyl, crizotinib, PF-06463922, homoharringtonine, Denileukin diftitox ontology, and LDK-378 (P<0.05). Conversely, a positive correlation was observed between the expression of *PPP4R1* and the IC50 value of fludarabine (P<0.05). This suggests that higher expression levels of *PPP4R1* are associated with increased resistance to fludarabine.

Predicting and constructing ceRNA regulatory networks

The importance of ceRNA regulatory networks in LIHC has been established by previous research. Hence, the process of forecasting and building ceRNA networks was carried out. The miRWalk and MicroT-CDS databases predicted a total of 122 and 199 miRNAs, respectively. The findings shown in *Figure 8A* demonstrated a group of miRNAs that were shared by both databases, specifically hsa-miR-320b, hsa-miR-1298-3p, hsa-miR-3120-3p, hsa-miR-5189-5p, hsa-miR-22-3p, hsa-miR-488-5p, hsa-miR-6738-3p, and hsa-miR-6738-3p. Further examinations of the connection between miRNAs and *PPP4R1* expression levels unveiled a noteworthy inverse relationship between hsa-miR-22-3p and *PPP4R1* in LIHC (R=−0.434, P<0.001).

Furthermore, the ENCORI and Lncbase databases were employed for the prediction of lncRNAs that targeted hsa-miR-22-3p, revealing predictions of 34 and 844 lncRNAs, respectively. *Figure 8B* displayed a group of lncRNAs, including AC021078.1, AC087741.1, AL008721.2, AL390294.1, FGD5 antisense RNA 1 (FGD5-AS1), GUSBP11, H19, LINC00963, NEAT1, NORAD, OIP5-AS1, SH3BP5-AS1, SNHG14, and SNHG29, which were found in both databases. Afterwards, the association between these 14 long non-coding RNAs (lncRNAs) and the level of expression of hsa-miR-22-3p was investigated. A total of 12 lncRNAs were found to have a negative correlation with hsa-miR-22-3p, specifically AC087741.1 (R=−0.393, P<0.001), AC021078.1 (R=−0.211, P<0.001), AL008721.2 (R=−0.408, P<0.001), FGD5-AS1 (R=−0.324,

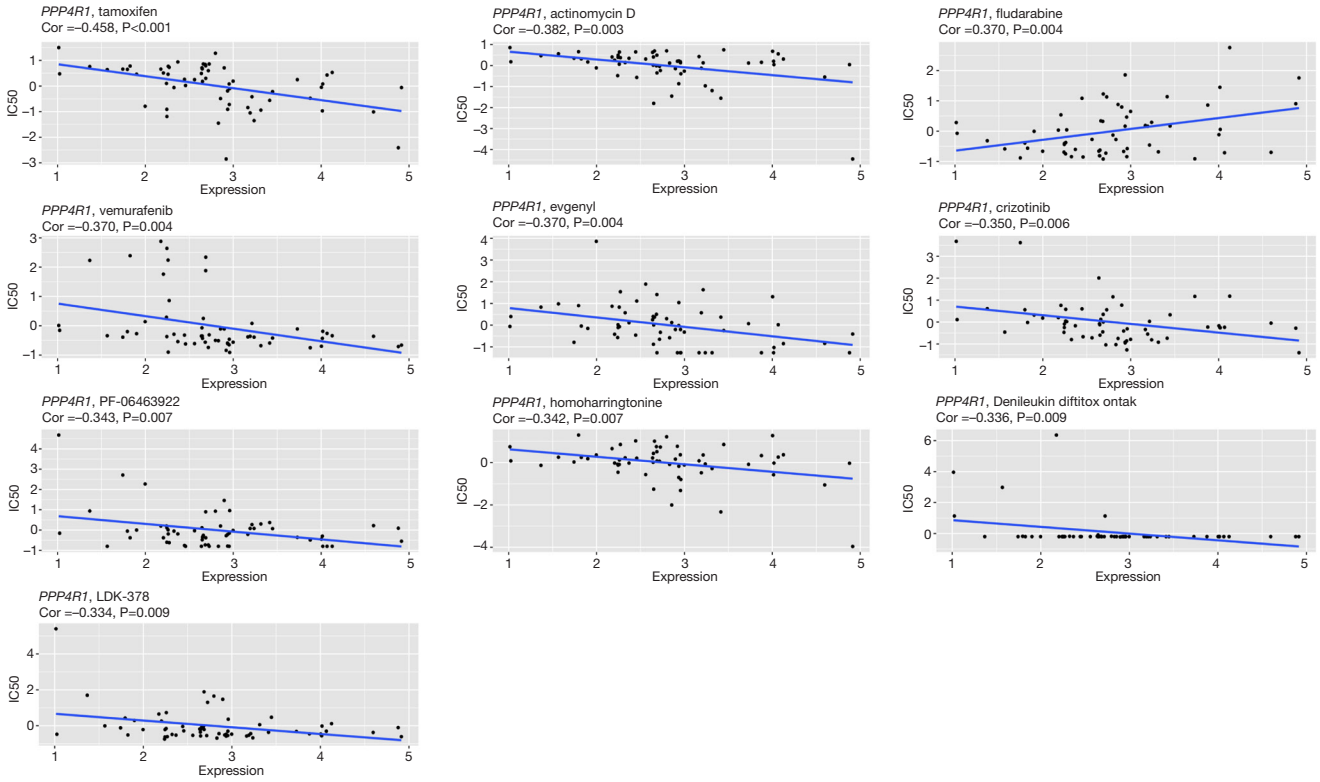

Figure 7 Scatterplots of correlation between *PPP4R1* expression levels and anti-cancer drugs. *PPP4R1*, protein phosphatase 4 regulatory subunit 1; IC50, half maximal inhibitory concentration.

P<0.001), GUSBP11 (R=−0.302, P<0.001), H19 (R=−0.238, P<0.001), NEAT1 (R=−0.117, P=0.025), NORAD (R=−0.217, P<0.001), OIP5-AS1 (R=−0.199, P<0.001), SH3BP5-AS1 (R=−0.179, P<0.001), SNHG14 (R=−0.383, P<0.001), and SNHG29 (R=−0.312, P<0.001) (*Figure 8C*) were observed. *Figure 8D* displays the maps of the ceRNA regulatory network.

In order to enhance the precision of the prediction, an analysis was conducted on the relationship between lncRNAs and *PPP4R1* in LIHC. The findings indicated that only FGD5-AS1 expression was increased, displaying a positive correlation with *PPP4R1*, and possessing diagnostic (AUC =0.774) and prognostic (HR =1.51, P=0.021) significance in LIHC (*Figure 8E*). The growth of LIHC may be influenced by the FGD5-AS1–hsa-miR-22-3p–*PPP4R1* ceRNA network, as suggested by these findings. *Figure 8F* displays the ultimate depiction of the ceRNA network.

Experimental verification

To validate the concordance between the *PPP4R1* expression level and the findings from TCGA data analysis, western blotting experiments was performed at the cellular level and IHC experiments was performed at the tissue level. The results of western blotting experiments demonstrated that the expression level of *PPP4R1* was elevated in HLE, Huh7, and HepG2 cells compared to that in LX-2 cells, however, *PPP4R1* is lowly expressed in PLC cells (*Figure 9A*). Then, image J software was used to calculate the gray value of *PPP4R1* expression in LIHC cells and hepatocytes, and a histogram was made (*Figure 9B*). IHC experiments analysis revealed a higher expression level of *PPP4R1* in tumor tissues than in paracancerous tissues (*Figure 9C,9D*), which aligns with the findings of TCGA analysis. To examine the cellular localization of *PPP4R1*, immunofluorescence experiments were conducted on LX-2, Huh7, and HLE cells. The results demonstrated that *PPP4R1* was predominantly localized in the cytoplasm and the cell membrane (*Figure 10*).

Discussion

Recent research indicates that the removal of phosphate

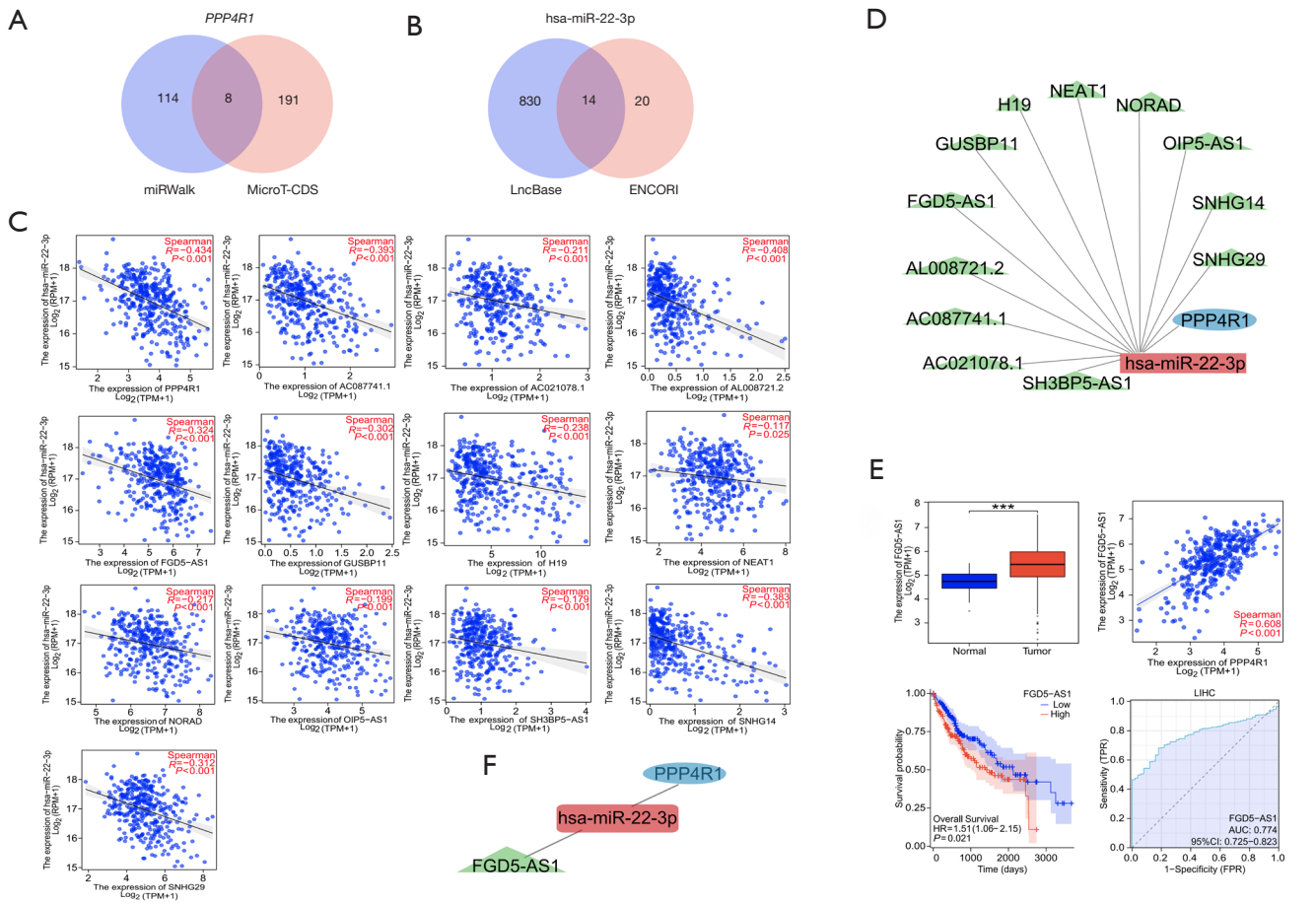

Figure 8 Prediction and construction of the ceRNA regulatory network of *PPP4R1*. (A) Venn diagram showing miRNAs targeting *PPP4R1* predicted by miRWalk database and MicroT-CDS database; (B) Venn diagram showing lncRNAs targeting hsa-miR-22-3p predicted by ENCORI database and LncBase database; (C) scatterplot of the correlation between *PPP4R1* and hsa-miR-22-3P as well as the correlation scatterplots of 12 lncRNAs with the hsa-miR-22-3P; (D) ceRNA regulatory network map; (E) box plot of FGD5-AS1 expression level, scatter plot of correlation between *PPP4R1* expression level and FGD5-AS1 expression level, Kaplan-Meier survival curve of FGD5-AS1, ROC curve of FGD5-AS1 in LIHC; (F) screened ceRNA regulatory network map. ***P < 0.001. ceRNA, competitive endogenous RNA; *PPP4R1*, protein phosphatase 4 regulatory subunit 1; miRWalk, mRNA-miRNA interactions; MicroT-CDS, mRNA-miRNA interactions; LncBase, miRNA-lncRNA interactions; ENCORI, encyclopedia of RNA interactomes; lncRNA, long non-coding RNA; FGD5-AS1, FGD5 antisense RNA 1; ROC, receiver operating characteristic; LIHC, liver hepatocellular carcinoma; RPM, reads per million; TPM, transcripts per million; TPR, true positive rate; FPR, false positive rate; AUC, area under the curve; CI, confidence interval.

groups from proteins raises the likelihood of tumor formation. One such example is the activation of the src homology-2 domain-containing protein tyrosine phosphatase-2 (SHP2) protein (17), which contains the src homology 2 domain and acts as a tyrosine phosphatase. This protein, encoded by PTPN11, significantly increases the susceptibility to leukemia in children and is now being targeted for cancer treatment. The primary role of *PPP4R1* is protein dephosphorylation, thus, increased *PPP4R1* expression may facilitate tumor advancement. Previous research has shown that *PPP4R1* expression is higher in lung cancer tissues compared to normal lung tissues, and it can enhance the migration and metastasis of NSCLC (6). The findings indicate that cancer therapy could potentially target *PPP4R1* as well.

In this research, the levels of *PPP4R1* expression were investigated in different cancer types, and its increase was observed in CHOL and LIHC. Additionally, through the

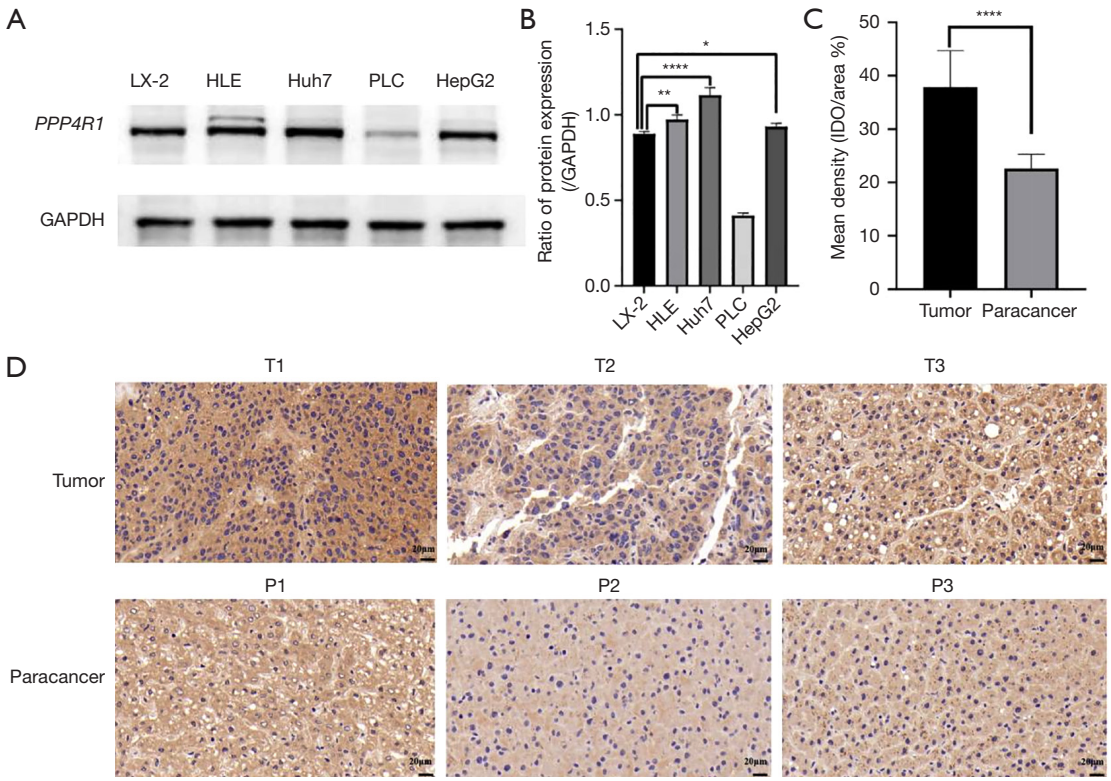

Figure 9 Western blotting and immunohistochemistry experiment. (A) The expression levels of *PPP4R1* in LX-2, HLE, Huh7, PLC and HepG2 were detected by western blotting assay; (B) statistical diagram of western blotting experiment; (C) statistical diagram of immunohistochemistry; (D) the expression level of *PPP4R1* in tumor tissues and adjacent tissues was detected by immunohistochemistry. Blue indicates nuclei, and tan indicates *PPP4R1* protein expression levels, with darker colours indicating higher expression levels and lighter colours indicating lower expression levels; scale length is 20 μm. *, P<0.05; **, P<0.01; ****, P<0.0001. *PPP4R1*, protein phosphatase 4 regulatory subunit 1; IOD, integrated optical density.

integration of clinical data, *PPP4R1* was found to have diagnostic value in 14 cancers and prognostic value in 5 cancers, but with both diagnostic and prognostic value only in LIHC. Consequently, subsequent investigations focused on elucidating the specific role of *PPP4R1* in LIHC. Clinical parameters indicated that *PPP4R1* was primarily linked to pathological stage, age, histological grade, and AFP level. AFP is a well-established diagnostic indicator for LIHC and is recognized for promoting growth, infiltration, spread, and evasion of the immune system (18,19). As a result, it has a vital function in the development and advancement of LIHC. Thus, it is plausible to suggest that *PPP4R1* might also facilitate the development and advancement of LIHC. The ROC curve indicated that *PPP4R1* exhibited a moderate diagnostic significance in LIHC. Consequently, utilizing *PPP4R1* and AFP in combination as a diagnostic indicator for LIHC might enhance the diagnostic precision of LIHC. According to the cox regression analysis, the prognosis in LIHC can be predicted independently by factors such as pathological stage, M stage, and *PPP4R1*. The findings offer valuable insights for the treatment and identification of LIHC in a clinical setting.

Furthermore, the GO enrichment analysis indicated that *PPP4R1* was primarily linked to cellular proliferation and the cell cycle. According to the KEGG enrichment analysis, the signaling pathways linked to *PPP4R1* primarily included PI3K-Akt, Wnt, AMPK, Hippo, and NF-κB, which have been demonstrated to facilitate the advancement of cancer (20-23). This implies that *PPP4R1* might also contribute to the progression of cancer. Furthermore, the KEGG enrichment analysis revealed a correlation between *PPP4R1* and NK cell-induced cytotoxicity, as well as PD-L1 expression within tumors and the PD-1 checkpoint pathway. These findings strongly suggest the potential involvement

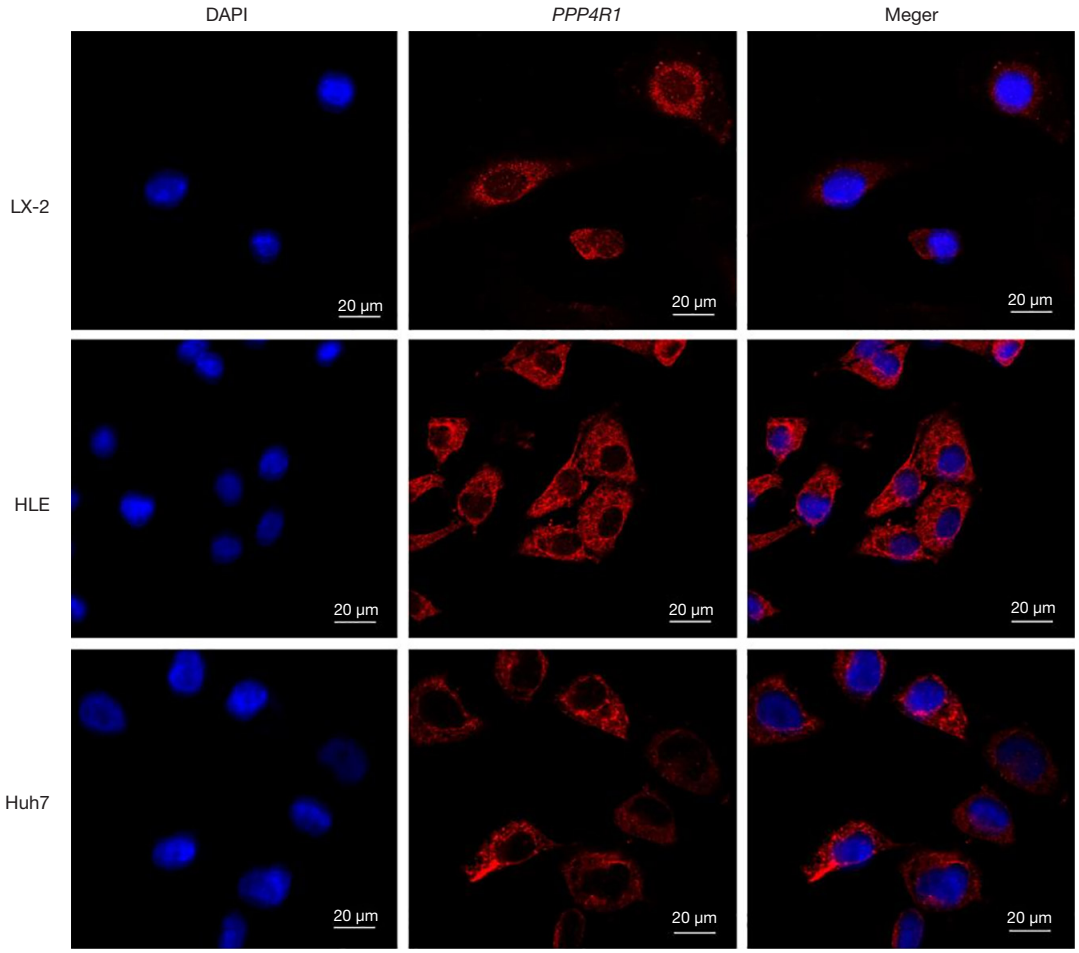

Figure 10 The localization of *PPP4R1* in LX-2 cell, HLE cell and Huh7 cell was detected by immunofluorescence staining. Blue indicates nucleus and red indicates *PPP4R1* protein; scale length is 20 μm. DAPI, 4',6-diamidino-2-phenylindole; *PPP4R1*, protein phosphatase 4 regulatory subunit 1.

of *PPP4R1* in immunotherapy. In order to further examine this hypothesis, an analysis of immune infiltration was performed in LIHC, revealing a strong association between *PPP4R1* and NK CD56bright cells. The results indicated that *PPP4R1* may have the ability to regulate NK cells in order to modify immunotherapy in tumors. Subsequent correlation analysis was conducted between *PPP4R1* and genes related to immunoinhibition, revealing a positive association between *PPP4R1* and PDCD1, HAVCR2, CTLA4, and TGF-β1. The PDCD1 gene produces PD-1 proteins in T cells, and the PD-1 receptor on T cells' surface can interact with PD-L1 ligands on tumour cells' surface, inhibiting T cell activity (24). Additionally, KEGG enrichment analysis revealed *PPP4R1*'s association with PD-1 and PD-L1 checkpoint signaling pathways, As PD-L1 has been shown to promote tumour immune escape (25), thus, *PPP4R1* might also facilitate immune evasion by tumour cells. Tim-3, also referred to as HAVCR2, was found to hinder the PI3K signaling pathway, consequently obstructing NK cell immune surveillance against LIHC cells and promoting their growth (26). This suggests that *PPP4R1* might play a role in regulating the immune function of NK cells, aligning with the KEGG enrichment analysis. CTLA4, a gene associated with checkpoints, has a crucial function in suppressing the activation of T cells and has been utilized as a focal point for tumor immunotherapy (27). Therefore, *PPP4R1* may also be a potential target for tumour immunotherapy. TGF-β1, the primary constituent of the TGF-β family, has been identified as a significant marker for the advancement of hepatitis C to cirrhosis and hepatocellular carcinoma (28).

The KEGG enrichment analysis findings indicated that *PPP4R1* was also linked to hepatitis C. Hence, *PPP4R1* might possess the potential to facilitate the progression of hepatitis C to hepatocellular carcinoma.

Following this, an analysis of drug sensitivity demonstrated a direct association between the *PPP4R1* expression level and the IC50 value of fludarabine. According to a prior investigation (29), it was found that fludarabine increased the harmful effects of NK cells on LIHC cells. Hence, combining fludarabine with NK cells during the treatment of LIHC patients might boost the effectiveness of therapy. Furthermore, the suppression of *PPP4R1* expression may lead to further improvements in therapeutic efficacy. The discovery highlights the role of *PPP4R1* in LIHC immunotherapy. Online databases were utilized to predict and construct ceRNA networks in order to identify upstream targets of *PPP4R1*. In conclusion, the ceRNA network consists of FGD5-AS1, hsa-miR-22-3p, and *PPP4R1*, with FGD5-AS1 and hsa-miR-22-3p identified as upstream targets of *PPP4R1*. According to a research, it was found that FGD5-AS1 contributes to the development of lenvatinib resistance in hepatocellular carcinoma (30), and *PPP4R1* is associated with fludarabine resistance, which implies that FGD5-AS1–hsa-miR-22-3p–*PPP4R1* ceRNA network might be linked to drug resistance in LIHC. Finally, experiments were conducted to verify the expression of *PPP4R1* protein in both cells level and tissues level. According to the western blotting experimental findings, the *PPP4R1* protein exhibited significant elevation in three LIHC cell lines (HLE, Huh7, and HepG2) in comparison to normal hepatocytes (LX-2). The experimental results from IHC also demonstrated a notable increase in *PPP4R1* expression in cancerous tissues when compared to adjacent paracancerous tissues. Furthermore, immunofluorescence experiments revealed that *PPP4R1* was present in both the cytoplasm and cell membrane. This finding further supports the potential of *PPP4R1* as an immunotherapeutic target for LIHC, as it is located on the cell membrane. These results indicate that *PPP4R1*, a cancer-causing gene, could potentially serve as a new indicator for LIHC.

This paper examined the mRNA and protein levels of *PPP4R1*, investigates its role in the clinic, and reveals its biological functions, drug sensitivity, and upstream targets. Nevertheless, the majority of these findings were anticipated based on publicly available information. Subsequent investigations will conduct cellular assays to delve deeper into the impact of *PPP4R1* on the characteristics of LIHC cells. To detect alterations in NK cell toxicity to LIHC cells, co-culturing of NK cells with LIHC cells will be conducted. The impact of fludarabine on apoptosis of LIHC cells will be assessed using flow cytometry. Using a dual luciferase reporter assay to verify the FGD5-AS1–hsa-miR-22-3p–*PPP4R1* ceRNA network.

Conclusions

To summarize, the research indicates a notable link between increased *PPP4R1* levels and the diagnosis of LIHC, as well as a negative outlook for the patient's prognosis. Moreover, this heightened manifestation could potentially lead to resistance against drugs and impede the effectiveness of immunotherapy in LIHC. Hence, targeting *PPP4R1* could be an innovative method for treating LIHC. The results offer valuable perspectives on the clinical treatment of patients with LIHC.

Acknowledgments

Funding: This work was supported by the National Natural Science Foundation of China (Nos. 81960519 and 82060514), Natural Science Foundation of Hainan Province (Nos. 2019CXTD406, 822RC700, and 2019RC204), Hainan Province Science and Technology Special Foundation (No. ZDYF2021SHFZ222), and the Research Project of Take off the Proclamation and Leadership of the Hainan Medical University Natural Science Foundation (No. JBGS202106).

Footnote

Reporting Checklist: The authors have completed the MDAR and REMARK reporting checklists. Available at https://tcr.amegroups.com/article/view/10.21037/tcr-23-1744/rc

Data Sharing Statement: Available at https://tcr.amegroups.com/article/view/10.21037/tcr-23-1744/dss

Peer Review File: Available at https://tcr.amegroups.com/article/view/10.21037/tcr-23-1744/prf

Conflicts of Interest: All authors have completed the ICMJE uniform disclosure form (available at https://tcr.amegroups.com/article/view/10.21037/tcr-23-1744/coif). The authors have no conflicts of interest to declare.

Ethical Statement: The authors are accountable for all aspects of the work in ensuring that questions related

to the accuracy or integrity of any part of the work are appropriately investigated and resolved. The study was conducted in accordance with the Declaration of Helsinki (as revised in 2013). The study was approved by Ethics Committee of the First Affiliated Hospital of Hainan Medical College (No. 2023-KYS-161) and informed consent was taken from all the patients.

References

1. Raja R, Wu C, Bassoy EY, et al. PP4 inhibition sensitizes ovarian cancer to NK cell-mediated cytotoxicity via STAT1 activation and inflammatory signaling. J Immunother Cancer 2022;10:e005026.
2. Walton J, Blagih J, Ennis D, et al. CRISPR/Cas9-Mediated Trp53 and Brca2 Knockout to Generate Improved Murine Models of Ovarian High-Grade Serous Carcinoma. Cancer Res 2016;76:6118-29.
3. Park J, Lee DH. Functional roles of protein phosphatase 4 in multiple aspects of cellular physiology: a friend and a foe. BMB Rep 2020;53:181-90.
4. Tikhonova A, Aifantis I. The taming of the NF-κB: PP4R1 navigates while PP4c dephosphorylates. Immunity 2012;37:594-6.
5. Hadweh P, Habelhah H, Kieff E, et al. The PP4R1 subunit of protein phosphatase PP4 targets TRAF2 and TRAF6 to mediate inhibition of NF-κB activation. Cell Signal 2014;26:2730-7.
6. Wang B, Pan LY, Kang N, et al. PP4R1 interacts with HMGA2 to promote non-small-cell lung cancer migration and metastasis via activating MAPK/ERK-induced epithelial-mesenchymal transition. Mol Carcinog 2020;59:467-77.
7. Xiang Y, Zong QB, Liu H, et al. lncRNA IGF2-AS regulates miR-500a-3p/PPP4R1/p-VEGFR2 signalling pathway to promote thyroid carcinoma progression and tubulogenesis. Clin Transl Med 2023;13:e1240.
8. Reinhold WC, Sunshine M, Liu H, et al. CellMiner: a web-based suite of genomic and pharmacologic tools to explore transcript and drug patterns in the NCI-60 cell line set. Cancer Res 2012;72:3499-511.
9. Liu J, Lichtenberg T, Hoadley KA, et al. An Integrated TCGA Pan-Cancer Clinical Data Resource to Drive High-Quality Survival Outcome Analytics. Cell 2018;173:400-416.e11.
10. Szklarczyk D, Kirsch R, Koutrouli M, et al. The STRING database in 2023: protein-protein association networks and functional enrichment analyses for any sequenced genome of interest. Nucleic Acids Res 2023;51:D638-46.
11. Yu G, Wang LG, Han Y, et al. clusterProfiler: an R package for comparing biological themes among gene clusters. OMICS 2012;16:284-7.
12. Ru B, Wong CN, Tong Y, et al. TISIDB: an integrated repository portal for tumor-immune system interactions. Bioinformatics 2019;35:4200-2.
13. Sticht C, De La Torre C, Parveen A, et al. miRWalk: An online resource for prediction of microRNA binding sites. PLoS One 2018;13:e0206239.
14. Paraskevopoulou MD, Georgakilas G, Kostoulas N, et al. DIANA-microT web server v5.0: service integration into miRNA functional analysis workflows. Nucleic Acids Res 2013;41:W169-73.
15. Li JH, Liu S, Zhou H, et al. starBase v2.0: decoding miRNA-ceRNA, miRNA-ncRNA and protein-RNA interaction networks from large-scale CLIP-Seq data. Nucleic Acids Res 2014;42:D92-7.
16. Karagkouni D, Paraskevopoulou MD, Tastsoglou S, et al. DIANA-LncBase v3: indexing experimentally supported miRNA targets on non-coding transcripts. Nucleic Acids Res 2020;48:D101-10.
17. Yuan X, Bu H, Zhou J, et al. Recent Advances of SHP2 Inhibitors in Cancer Therapy: Current Development and Clinical Application. J Med Chem 2020;63:11368-96.
18. Zheng Y, Zhu M, Li M. Effects of alpha-fetoprotein on the occurrence and progression of hepatocellular carcinoma. J Cancer Res Clin Oncol 2020;146:2439-46.
19. Zhang M, Liu K, Zhang Q, et al. Alpha fetoprotein promotes polarization of macrophages towards M2-like phenotype and inhibits macrophages to phagocytize hepatoma cells. Front Immunol 2023;14:1081572.
20. Paskeh MDA, Ghadyani F, Hashemi M, et al. Biological impact and therapeutic perspective of targeting PI3K/Akt signaling in hepatocellular carcinoma: Promises and Challenges. Pharmacol Res 2023;187:106553.
21. He S, Tang S. WNT/β-catenin signaling in the development of liver cancers. Biomed Pharmacother

2020;132:110851.
22. Cui J, Shen HM, Lim LHK. The Role of Autophagy in Liver Cancer: Crosstalk in Signaling Pathways and Potential Therapeutic Targets. Pharmaceuticals (Basel) 2020;13:432.
23. Shi H, Zou Y, Zhong W, et al. Complex roles of Hippo-YAP/TAZ signaling in hepatocellular carcinoma. J Cancer Res Clin Oncol 2023;149:15311-22.
24. Palamarchuk A, Tsyba L, Tomasello L, et al. PDCD1 (PD-1) is a direct target of miR-15a-5p and miR-16-5p. Signal Transduct Target Ther 2022;7:12.
25. Suresh S, Chen B, Zhu J, et al. eIF5B drives integrated stress response-dependent translation of PD-L1 in lung cancer. Nat Cancer 2020;1:533-45.
26. Tan S, Xu Y, Wang Z, et al. Tim-3 Hampers Tumor Surveillance of Liver-Resident and Conventional NK Cells by Disrupting PI3K Signaling. Cancer Res 2020;80:1130-42.
27. Russell BL, Sooklal SA, Malindisa ST, et al. The Tumor Microenvironment Factors That Promote Resistance to Immune Checkpoint Blockade Therapy. Front Oncol 2021;11:641428.
28. Hamad RS, Al Abdulsalam NK, Elrefaiy MA, et al. Interplay between TGF-b1 and miRNA-122 biomarkers in hepatocellular carcinoma progression in patients with chronic hepatitis C. Trop Biomed 2022;39:559-68.
29. Meng G, Fei Z, Fang M, et al. Fludarabine as an Adjuvant Improves Newcastle Disease Virus-Mediated Antitumor Immunity in Hepatocellular Carcinoma. Mol Ther Oncolytics 2019;13:22-34.
30. Song M, Ma L, Shen C, et al. FGD5-AS1/miR-5590-3p/PINK1 induces Lenvatinib resistance in hepatocellular carcinoma. Cell Signal 2023;111:110828.

Cite this article as: Li X, Pan Y, Feng S, Xing W, Lin B, Li W, Li M, Zhu M. The diagnostic, prognostic, drug sensitivity and ceRNA internet of *PPP4R1* in liver hepatocellular carcinoma (LIHC). Transl Cancer Res 2024;13(2):594-612. doi: 10.21037/tcr-23-1744

